ARTICLE

Computerized FDTD Method for Longitudinal Optical Phonon Energy on Semiconductor Hybrid Structure for High Power Devices Fabrication

Phyo Sandar Win[1]   Hsu Myat Tin Swe[1]   Hla Myo Tun[2*]

1.Department of Electronic Engineering, Technological University (Taungoo), Bago, Myanmar
2.Faculty of Electrical and Computer Engineering, Yangon Technological University, Yangon, Myanmar

ABSTRACT

The research problem in this study is the longitudinal optical phonon energy on metal/semiconductor interface for high performance semiconductor device. The research solution is to make the software model with finite difference time domain (FDTD) solution for transmission and reflection pulse between metal and semiconductor interface for carrier dynamics effects. The objective of this study is to find the quantum mechanics understanding on interface engineering for fabricating the high performance device for future semiconductor technology development. The analysis was carried out with the help of MATLAB. The quantum mechanical spatial field on metal-semiconductor stripe structure has been analyzed by FDTD techniques. This emission reveals a characteristic polar radiation distribution of electric dipoles and a wavelength independent of the structure size or the direction of emission; consequently, it is attributed to thermally generate electric dipoles resonating with the longitudinal optical phonon energy. Phonon energy occurs lattice vibration of material by the polarization of light, if the material has rigid structure reflect back the incident light. So, high reflective metal-semiconductor structure always use as photodectors devices in optical fiber communication. No lattice vibration material structure has no phonon effect, so this structure based devices can get high performance any other structure based devices. The transmission and reflection coefficient of metal-semiconductor GaN/Au layer structure compare with GaN/Ti and GaN/Pt structure. Parallel (P) and transverse (S) polarization of light incident on a metal-semiconductor nanolayer structure with IR wavelength. Efficient use of the layer by layer (LbL) method to fabricate nanofilms requires meeting certain conditions and limitations that were revealed in the course of research on model systems.

1. Introduction

The FDTD method is one of the most widely used methods in electromagnetic simulation. Finite-difference time-domainor Yee's method is a numerical analysis technique used for modeling computational electrodynamics and it has recently been applied to the simulation of the Schrödinger equation. In principle, the approaches can be divided into three groups: (i) crystal defects (nitrogen vacancies, nitrogen interstitials, gallium vacancies, etc.)

Corresponding Author:
Hla Myo Tun,
Faculty of Electrical and Computer Engineering, Yangon Technological University, Yangon, Myanmar;
Email: hlamyotun@ytu.edu.mm

mediating magnetic ordering over the crystal from one magnetic center to another; (ii) presence of free charge carriers in the materials and co-doping with donors and (iii) coupling of the separated magnetic moments with magnetically neutral impurities (e.g., oxygen) which results in overall magnetic order in the scheme [1].

Recently, semiconductor researches are more attractive than other research fields. Semiconductor devices employ the charge of the carriers to achieve the desired functionality. Since it is a time-domain method, FDTD solutions can cover a wide frequency range with a single simulation run, and treat nonlinear material properties in a natural way. This technique allows for the simulation of laser excitation dynamics as well as for the determination of energy eigenstates [2].

Semiconductor devices have attracted great attention due to the quantization of carriers in three dimensions, leading to discrete spectra. Among other things, they present the possibility of studying the details interaction of particles in a controlled environment. The advent of measurement techniques, such as single-electron capacitance spectroscopy (SECS), has made possible determination of the energy of individual particles. The finite-difference time-domain method is arguably the simplest both conceptually and in terms of implementation of the full-wave techniques used to solve problems in electromagnetic. The FDTD method requires the discretization of time and space.

2. Materials and Methods

2.1 Implementation of Absorption by Fresnel Equation

The samples are undoped metal/semiconductor stripe structure. In this metal-semiconductor layer stripe structure, materials, thickness, refractive index (n) and extinction coefficient (k) values are shown in simulation results respectively.

In this paper, p-polarized light is incident on metal layer and then is compared with the reflectivity values for three types of metal-semiconductor structure to get the less phonon effect high performance layer structure.

The Fresnel equations describe the reflection and transmission of light when light is incident on an interface between different optical media. When light travelling in a denser medium strikes the surface of a less dense medium (that is, $n_1 > n_2$) beyond a particular incidence angle known as the critical angle, all light is reflected and $R_s = R_p = 1$.

P-polarized light:

$$r_p = \frac{n_i \cos(\theta_t) - n_t \cos(\cos\theta_i)}{n_i \cos(\theta_t) + n_t \cos(\theta_i)} \qquad \text{Equation (1)}$$
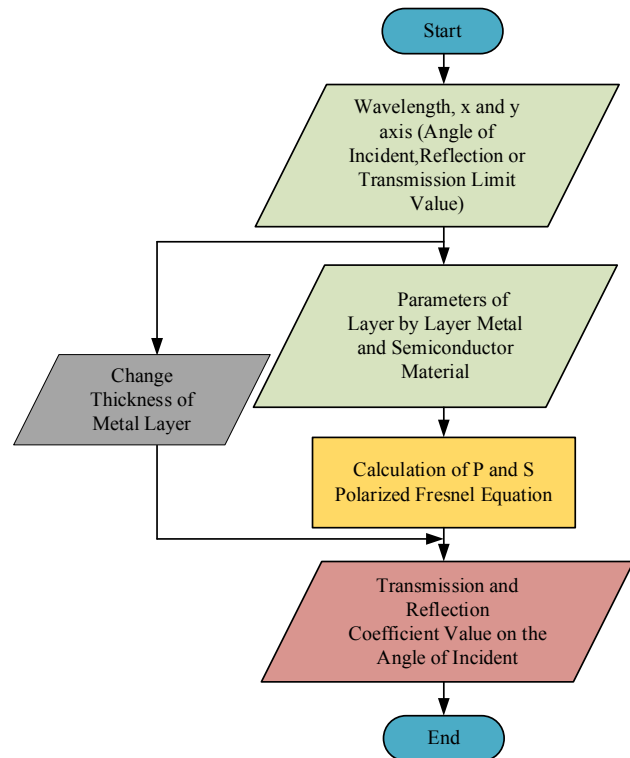
Figure 1. Flowchart of Transmission and Reflection Coefficient

$$t_p = \frac{2n_i \cos(\theta_i)}{n_i \cos(\theta_t) + n_t \cos(\theta_i)} \qquad \text{Equation (2)}$$

S-polarized light:

$$r_s = \frac{n_i \cos(\theta_i) - n_t \cos(\theta_t)}{n_i \cos(\theta_i) + n_t \cos(\theta_t)} \qquad \text{Equation (3)}$$

$$t_s = \frac{2n_i \cos(\theta_i)}{n_i \cos(\theta_i) + n_t \cos(\theta_t)} \qquad \text{Equation (4)}$$

For both polarization,

$$n_i \sin(\theta_i) = n_t \sin(\theta_t) \qquad \text{Equation (5)}$$

nall is a software for the simulation of surface plasmon resonance curves, transmission and reflection coefficient curves by polarizations based on the Fresnel formalism. Absorption value can be obtained by substration the value of reflection and transmission value from one.

2.2 Implementation of Reflection Analysis on FDTD Measurement

Figure 2 illustrates the flowchart of reflection analysis

between metal and semiconductor interface with MUR and PML boundary. At first, the boundary condition of MUR and PML with suitable courant factor is initialized. After that, the permittivity, permeability, speed of light and wavelength of free space parameter and specific time steps for FDTD is declared. The physical parameters for metal layer and semiconductor layers are specified. The two-dimensional finite difference time domain (2D FDTD) algorithm is initialized.

And then the boundary condition of MUR and PML is calculated. Finally, the reflection pluses for boundary condition of MUR and PML are displayed.

2.3 Implementation of Transmission Analysis on FDTD Measurement

Figure 3 illustrates the flowchart of transmission analysis between metal and semiconductor interface with MUR and PML boundary.
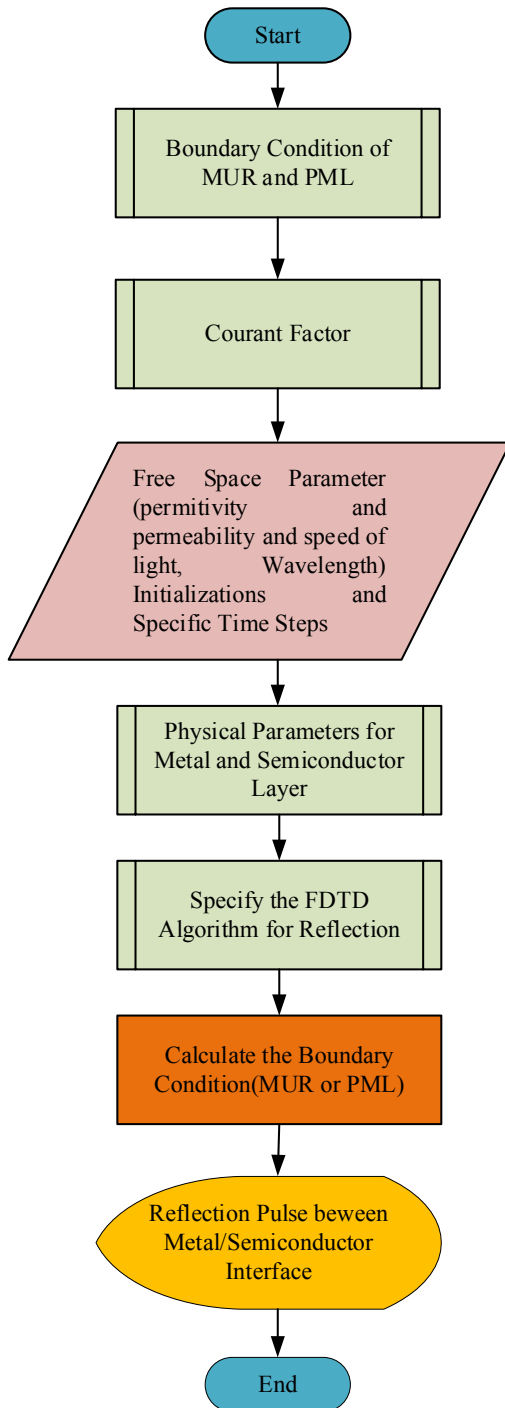
Figure 2. Flowchart for Reflection Analysis
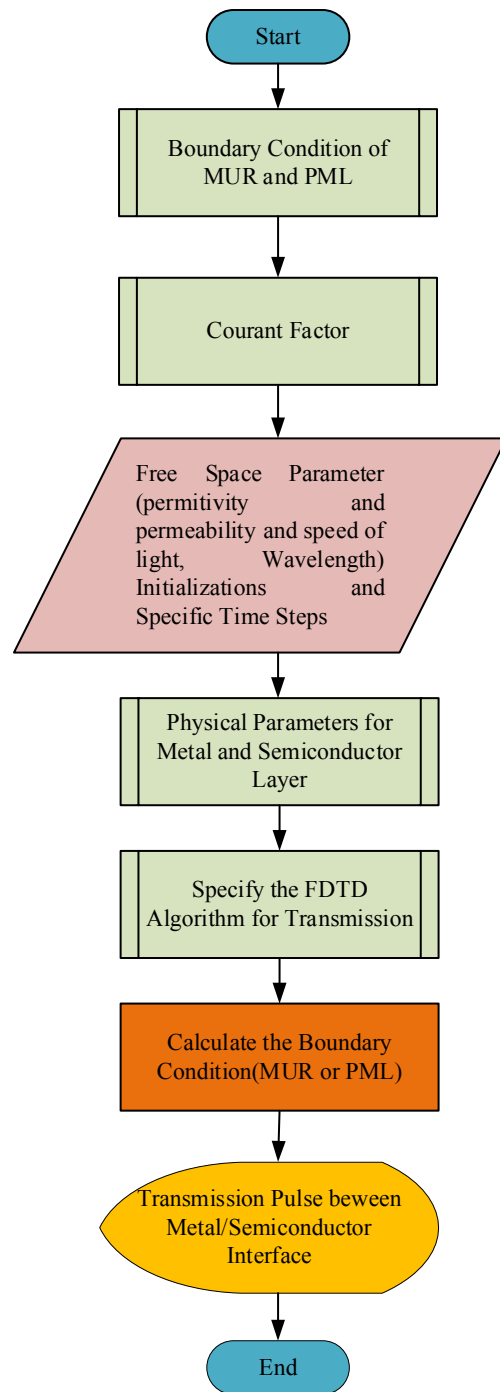
Figure 3. Flowchart for Transmission Analysis

At first, the boundary condition of MUR and PML with appropriate courant factor is reset. Afterward, the permittivity, permeability, speed of light and wavelength of free space parameter and specific time steps for FDTD is professed. The corporeal parameters for metal layer and semiconductor layers are quantified. The two-dimensional finite difference time domain (2D FDTD) process is modified. And then the boundary condition of MUR and PML is premeditated. Lastly, the transmission pluses for boundary condition of MUR and PML are exhibited.

2.4 Implementation of Electric Field and Electric Flux Density FDTD Measurement

All material is made up of charged particles. The material may be neutral overall because it has as many positive charges as negative charges. Nevertheless, there are various ways in which the positive and negative charges may shift slightly within the material, perhaps under the influence of an electric field. The resulting charge separation will have an effect on the overall electric field. Because of this it is often convenient to introduce a new field known as the electric flux density D which has units of Coulombs per square meter (C/m^2). The D field ignores the local effects of charge which is bound in a material [3]. In free space, the electric field and the electric flux density are related by

$$D = \varepsilon_0 E \qquad \text{Equation (6)}$$

Gauss's law states that integrating D over a closed surface yields the enclosed free charge.

$$\oint_S D.ds = Q_{enc} \qquad \text{Equation (7)}$$

Where S is the closed surface, ds is an incremental surface element whose normal is directed radically outward, and Q_{enc} is the enclosed charge. Taking S to be a spherical surface with the charge at the center, it is simple to perform the integral.

$$\oint_S D.ds = \int_{\theta=0}^{\pi} \int_{\varphi=0}^{2\pi} \varepsilon_0 \frac{Q_1}{4\pi\varepsilon_0 r^2} \hat{a}_r.\hat{a}_r r^2 \sin\theta d\varphi d\theta = Q_1$$

$$\text{Equation (8)}$$

The samples were undoped (u-) metal/semiconductor stripe structures. The semiconductor films with the thickness of 0.1 μm were grown by a metal organic vapour phase epitaxy on n-type doped (n-) (100) conventional substrate. The stripe width values of semiconductor and metal were variable micro-meter (μm). The geometric

configurations for FDTD measurement on the metal/semiconductor stripe structure is shown in Figure 4.
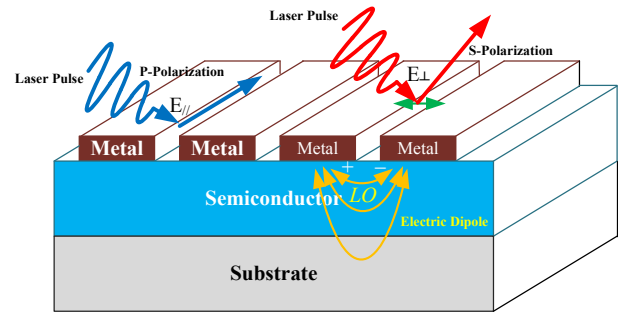
Figure 4. Geometric Configurations

The result is actually independent of the surface chosen, but the integral is especially easy to perform for a spherical surface. The integral in Equation (7) is always equal to the enclosed charge as it does in frees pace. However, things are more complicated when material is present. Two large parallel plates carry uniformly distributed charge of equal magnitude but opposite sign. The dashed line represents an integration surface S which is assumed to be sufficiently far from the edges of the plate so that the field is uniform over the top of S. This field is identified as E_0. The fields are zero outside of the plates and they are tangential to the sides of S within the plates. Therefore, the only contribution to the integral is from the top of S. The result of the integral HS .E0 .ds is the negative charge enclosed by the surface. Figure 5 shows the results of FDTD simulation for the simulation model of the electric field.
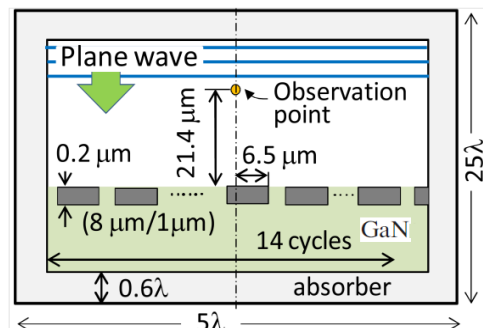
Figure 5. Simulation Model Using the FDTD Method

When a light wave packet with 10 cycles of oscillation (approximately 1 ps duration) and a low electric field amplitude of 3×10^3 V/cm, is incident on the sample for (a) polarization direction E parallel stripe and (b) E perpendicular stripe. The geometric condition including the observation point of the electric field is exhibited in the inset of Figure 5.

2.5 Quantum Mechanical Model

The conventional device modelling pilots to two im-

portant inaccuracies pertains to the carrier concentration near the semiconductor surface. Initially, the dividing of the conduction band into quite a few discrete eigenvalues is not measured. That goes ahead to an over evaluation of the surface charge as the energy difference between those discrete eigenvalues and the fermi-level is superior than the one from the bottom of the conduction band to the fermi-level. Next, the conventional models do not regard as that the shape of the wave function diminishes the carrier concentration near the semiconductor surface as well. Therefore, a meticulous approach to imitate the carrier concentration has to make sure of both effects by contributing the rough calculation for the wave function and the actual band structure of semiconductor devices.

2.5.1 Approach to Wave Approximation

The first quantum mechanical effects by a diminution of the density of states near the semiconductor interface affecting an exponential shape function is called wave function approximation. This pursues an approach proposed by [4],

$$SD(i) = SD\left(1 - e^{-(i-i_0)^2/\lambda_{Thermal}}\right) \qquad \text{Equation (9)}$$

Where 'i' is the distance to the semiconductor interface and 'i_0' is an offset to match the nonzero carrier concentration near the surface stanching from the finite barrier height. $\lambda_{Thermal}$ is the thermal wavelength conscientious for the lessening of the quantum mechanical effects with increasing distance from the semiconductor interface.

$$\lambda_{Thermal} = \frac{\sqrt{2mkT}}{h} \qquad \text{Equation (10)}$$

If that improvement is utilized the qualitative carrier distribution near the semiconductor interface in physically powerful inversion which is duplicated quite well but devoid deliberation of band structure effects is not the issue in the threshold level region [5].

2.5.2 Approach to Energy Band Structure Approximation

Near the surface of the lowest eigenenergy is connotation higher than the band edge thus reasoning an over evaluation of the charge when the conventional imitation approach is utilized. The essential initiative of the current model is to substitute the effective band edge by the first discrete energy level. This appears realistic as quantum mechanical computations confirm that regularly more than 95% of the carriers are in that energy band. The band edge

at the semiconductor surface is set to:

$$E_{g,Semicon\ Surface}^{QMM} = E_{g,Semicon\ surface}^{Conventional} + \Delta E_g \qquad \text{Equation (11)}$$

Whereas $E_{g,Semicon\ Surface}^{QMM}$ is the developed bandgap energy which is utilized in the Boltzmann stistics, $E_{g,Semicon\ Surface}^{Conventional}$ is the bandgap in accordance with the material specification and ΔE_g is the applied modification. The current model attaches the band edge $E_{g,Semicon\ Surface}^{QMM}(i)$ surrounded by the device to the value of $E_{g,Semicon\ Surface}^{QMM}$ as long as $E_{g,Semicon\ Surface}^{QMM} > E_{g,Semicon\ Surface}^{Conventional}(i)$..

he accurate computation of the first energy level is numerically expensive and ssitates the explanation of the Schrodinger equation and estimation is utilized. The offset ΔE_g is estimated subsequent aestablishment of Van Dort et al [6-9] which reads as

$$\Delta E_g = \frac{13}{9}\beta\left(\frac{\in}{4qkT}\right)^{1/3}\left|E_{semicon\ surface}\right|^{2/3} \qquad \text{Equation (12)}$$

reas $\left|E_{semicon\ surface}\right|$ is the magnitude of the electric field at the semiconductor interface and $\in$ is the permittivity of the semiconductor, $\beta = 4.1 \times 10^{-8}$ eVcm is an empirical constant.

3. Results and Discussions

3.1 Winspall Analysis on Metal-Semiconductor Nanolayer Structure

Winspall is a software for the simulation of surface plasmon resonance curves, transmission and reflection coefficient curves by polarizations based on the Fresnel formalism. A laser beam is reflected from the surface of the material layer and the reflected light is collected as a function of the angle of incidence.
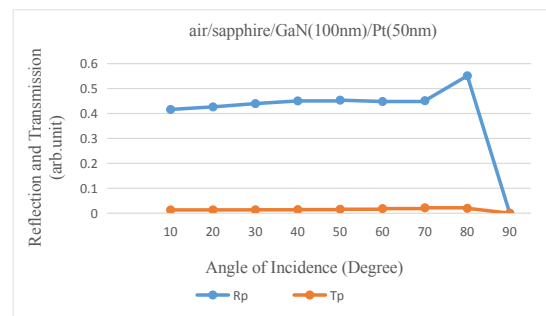
Figure 6. Reflection and Transmission Coefficient, λ=690 nm,Air(n=1,k=0, Thickness=0)/Sapphire(n=1.76, k=0,Thickness=100 nm)/GaN(n=2.365,k=0, Thickness=100 nm)/Pt(n=2.51,k=4.43,Thickness=50 nm)

Figure 6 shows the transmission and reflection coefficient value for air/sapphire/GaN /Platinum (Pt) structure. Reflection coefficient value of nearly 0.42 (arb.unit) and transmission coefficient value of 0.015 (arb.unit) obtain p-polarized light incident on this structure I. Nearly 0.42 reflection coefficient value is obtained along the incident angle 10 to 70 degree but the greater the angle of 70 degree, the higher the reflection coefficient value as shown in Figure 6.
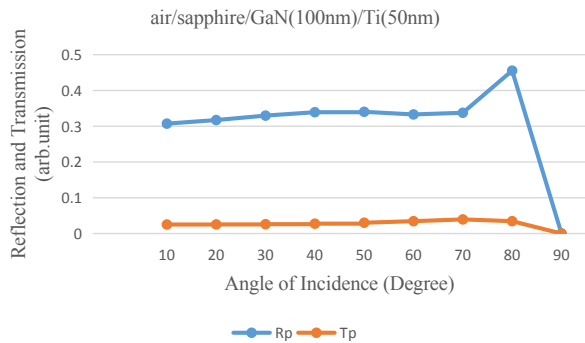
Figure 7. Reflection and Transmission Coefficient, λ=690 nm,Air(n=1,k=0, Thickness=0)/Sapphire(n=1.76,k=0,Thickness=100nm)/GaN(n=2.365, k=0, Thickness=100 nm)/Ti(n=3.03,k=3.65,Thickness=50 nm)

Figure 7 shows the transmission and reflection coefficient value for air/sapphire/GaN/Titanium (Ti) structure. Reflection coefficient value of nearly 0.31 (arb.unit) and transmission coefficient value of 0.03 (arb.unit) obtain p-polarized light incident on this structure II.
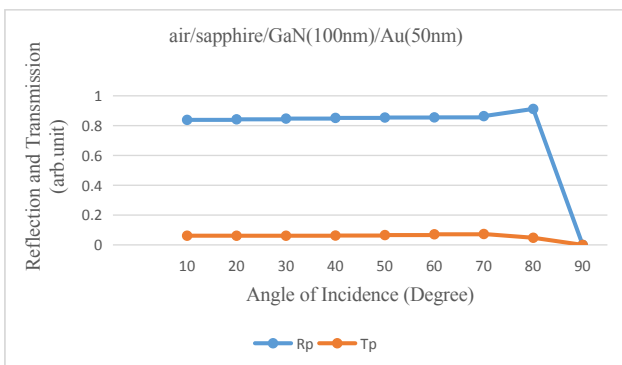
Figure 8. Reflection and Transmission Coefficient, λ=690 nm, Air (n=1,k=0, Thickness=0)/Sapphire(n=1.76,k=0,Thickness=100 nm) /GaN (n=2.365, k=0, Thickness=100 nm)/Au(n=0.16,k=3.80,Thickness=50 nm)

Nearly 0.31 reflection coefficient value is obtained along the incident angle of 10 to 70 degree but the greater the angle of 70 degree, the higher the reflection coefficient value as shown in Figure 8. Lower reflection coefficient value and a little higher transmission coefficient value in structure II compared with the structure I. So, structure II has high phonon effect than structure I.

Figure 8 shows the transmission and reflection coefficient value for air/sapphire/GaN/Gold(Au) structure. Reflection coefficient value of nearly 0.85 (arb.unit) and transmission coefficient value of 0.06 (arb.unit) obtain p-polarized light incident on this structure III. Nearly 0.85 reflection coefficient value is obtained along the incident angle of 10 to 70 degree but the greater the angle of 70 degree, the higher the reflection coefficient value as shown in Figure 8.
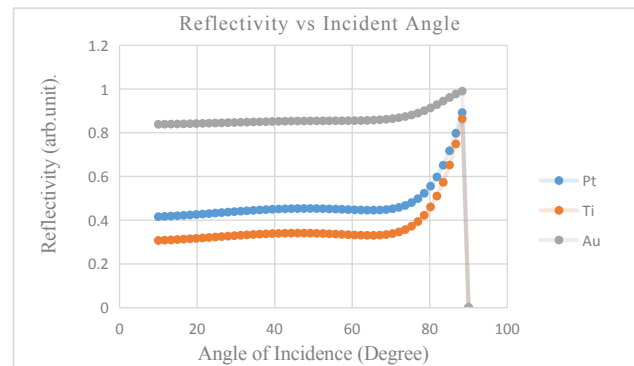
Figure 9. Comparison of Reflectivity for Au, Pt and Ti Metal
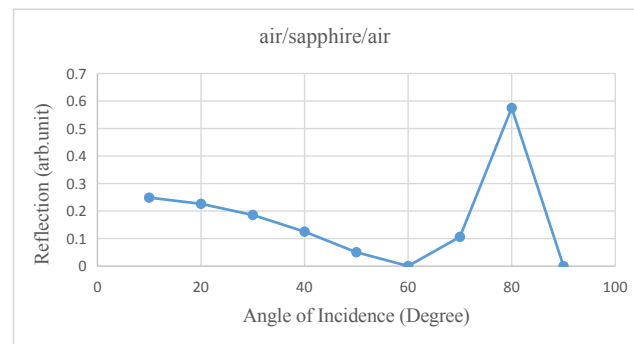
Figure 10. Reflection Coefficient, λ=632.8 nm, Air(n=1,k=0,Thickness=0) /Sapphire(n=1.76,k=0,Thickness=100 nm)

Highest reflection coefficient value is obtained in this structure III compared with the other two structures as shown in Figure 9. Structure III has less phonon effect than the other two structures, so this structure is very suitable to use in high performance metal-semiconductor based optical semiconductor devices. The following results show the step by step layer structure for structure III.

In Figure 10, layer 1 is air (n=1, k=0) so thickness is zero. Layer 2 is 100 nm thick Al_2O_3 sapphire substrate (n=1.77, k=0) with the wavelength of 632.8 nm. Reflection coefficient is zero about 58 degree to 63 degree and then more and more light is reflected until 90 degree.
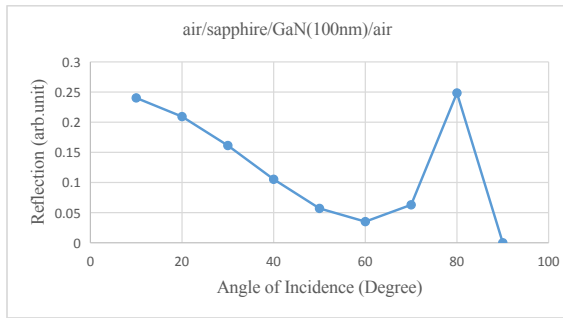
Figure 11. Reflection Coefficient, λ=632.8 nm, Air (n=1, k=0, Thickness=0) /Sapphire(n=1.76, k=0,Thickness=100 nm)/ GaN (n=2.37966,k=0, Thickness=100 nm)
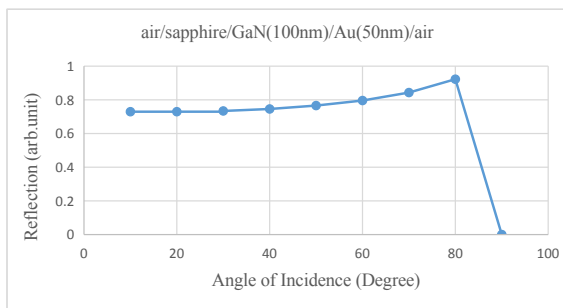
Figure 12. Reflection Coefficient, λ=632.8 nm, Air(n=1,k=0,Thickness=0) /Sapphire(n=1.76,k=0,Thickness=100 nm)/GaN(n=2.3796,k=0,Thickness=100 nm)/ Au((n=0.18104,k=3.0681,Thickness=50 nm)

In Figure 11, a 100 nm thick GaN layer is added on top of the substrate. Zero reflection coefficient value is lost because GaN layer is coated onto the substrate. Lower reflection coefficient value is obtained about nearly 70 degree but reflection coefficient value is steadily high from about 75 degree to 90 degree. Highest reflection coefficient value can get near the 90-degree p-polarized incident light. In Figure 12, a 50 nm thick gold (Au) layer is now coated on the layer of GaN. Higher reflection coefficient value is obtained in this structure.
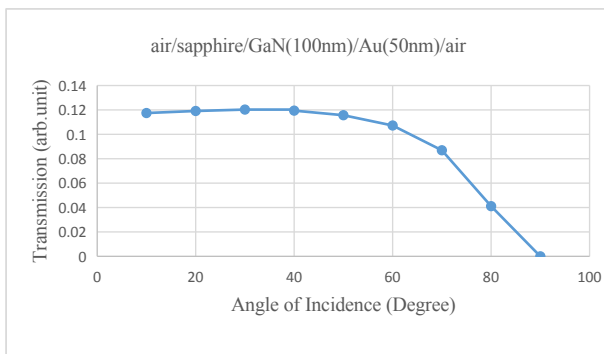
Figure 13. Transmission Coefficient, λ=632.8 nm, Air (n=1, k=0, Thickness=0) /Sapphire(n=1.76, k=0,Thickness=100 nm)/GaN(n=2.3796,k=0,Thickness =100 nm)/ Au(n=0.18104,k=3.0681,Thickness=50 nm)
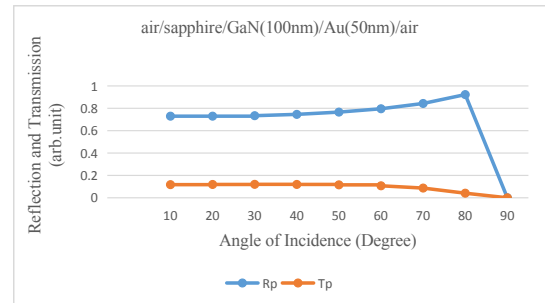
Figure 14. Transmission and Reflection Coefficient, λ=632.8 nm,Air(n=1,k=0, Thickness=0)/Sapphire(n=1.76,k=0,Thickness=100 nm)/GaN(n=2.37966, k=0,Thickness=100 nm)/ Au(n=0.18104,k=3.0681,Thickness=50 nm)

In Figure 13 shows transmission coefficient of the air / sapphire/ GaN / Au/ air structure. Transmission coefficient value is nearly 0.12 until 45 degree and then transmission coefficient is gradually decreased to zero until 90 degree. The higher the reflection value, the lower the transmission value, as shown in Figure 12 and Figure 13. Figure 14 illustrates transmission and reflection coefficient of p-polarization light in air/substrate/GaN/Au/air structure. According to Figure 14, reflection coefficient is more and more increased until total internal reflection. At that time transmission coefficient is closed to zero above 65 degree.
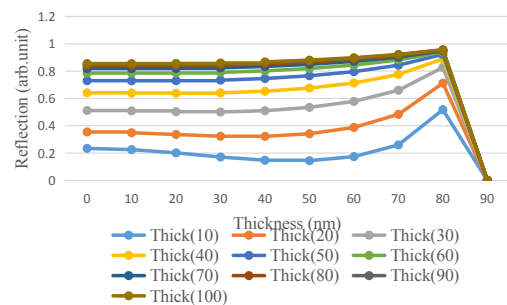
Figure 15. Reflection Coefficient, λ=632.8 nm, Air(n=1,k=0,Thickness=0)/ Sapphire(n=1.76,k=0,Thickness=100 nm)/GaN(n=2.37966,k=0,Thicknes s=100 nm)/ Au(n=0.18104,k=3.0681,Thickness=10 nm to 100 nm)
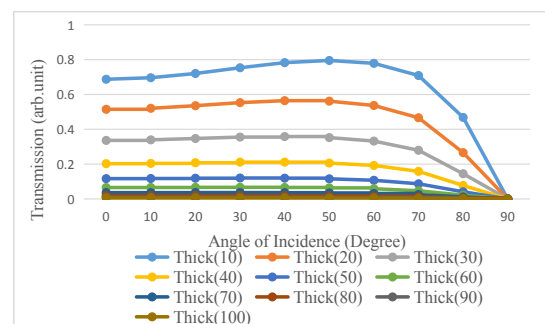
Figure 16. Transmission Coefficient, λ=632.8 nm, Air (n=1,k=0,Thickness=0) /Sapphire (n=1.76,k=0,Thickness=100 nm)/GaN(n=2.37966,k=0,Thicknes s=100 nm)/ Au(n=0.18104, k=3.0681,Thickness=10 nm to 100 nm)

Figure 15 shows the reflection coefficient values for top layer gold (Au) thickness are changed from 10 nm to 100 nm. The greater the thickness, the higher the reflection coefficient is obtained. According to the simulation result, top metal layer thickness value of 100 nm (0.1um) obtains high reflectivity value. Figure 16 illustrates the value of transmission coefficient for air/ sapphire/GaN/Au/air structure. The greater the thickness, the lower the transmission coefficient is obtained. So, above 0.1 um thick of metal layer should be used in high performance metal-semiconductor based semiconductor devices.

3.2 Transmission, Reflection and Absorption Analysis on P-Polarized Incident Angle

Reflection, Transmission and Absorption values for air/ sapphire/GaN/Au/air structure along the angle of incidence 10 to 90 degrees is shown in Figure 17.
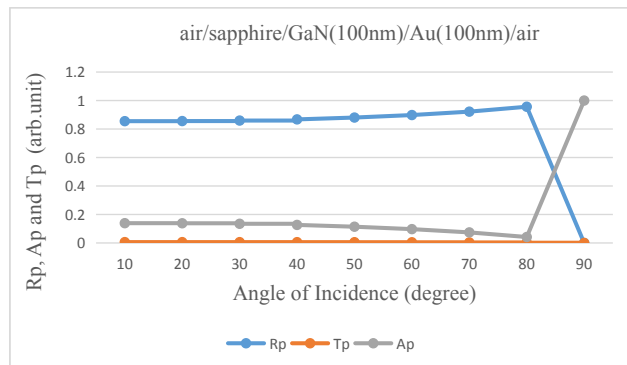
Figure 17. Reflection, Transmission and Absorption Analysis

When the reflection value is high, lower transmission and absorption value are obtained in this structure. Low absorption is less phonon energy for this structure. Along the angle of incidence, 80 degree incident light is the highest reflection value otherwise this condition gets low absorption rate.

3.2.1 Analysis on Thickness of Materials

The p-polarization of light 80 degree is incident on this M-S structure. The thickness of Au (10 nm to 100 nm) metal changes result is shown in Figure 18. 100 nm thick Au metal has high reflection value. Transmission value is zero and absorption value is nearly 0.03. So, 100 nm or upper thickness of Au metal layer can be used in high performance device (for less phonon effect).

The semiconductor GaN (10 nm to 100 nm) layer thickness changes result is shown in Figure 19.
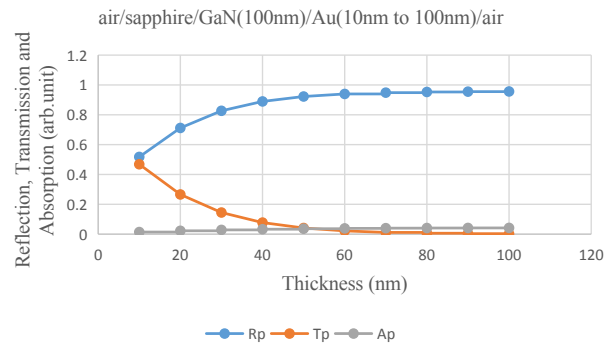
Figure 18. Reflection, Transmission and Absorption Analysis of Metal Layer
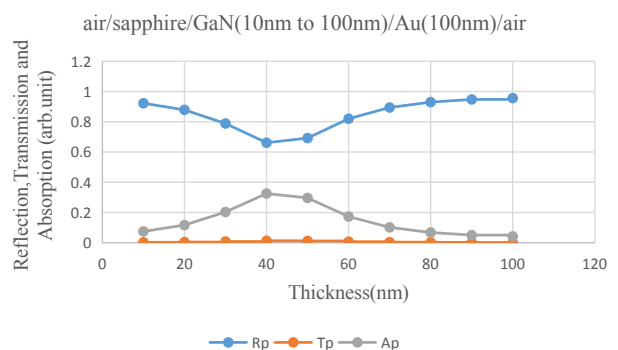
Figure 19. Reflection, Transmission and Absorption Analysis of Semiconductor Layer

Inversely proportional of reflection and absorption values can be seen in this result. Transmission value is nearly zero value in this condition. So, 100 nm or upper thickness of GaN semiconductor layer should be used in high performance device (for less phonon effect).

3.2.2 Absorption Analysis on IR Wavelength

Figure 20 illustrates the absorption coefficient value in visible wavelength region (400-700 nm).
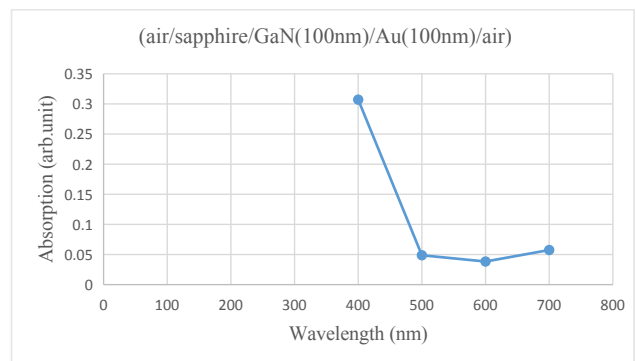
Figure 20. Absorption Analysis on 400-700 nm Wavelength

In 400 nm, 80-degree incident light, absorption coeffi-

cient value is about 0.31. In 500 nm, absorption coefficient value is about 0.05. In 600 nm, absorption coefficient value is about 0.04. In 700 nm, absorption coefficient value is about 0.0625. Less absorption rate gets about 600 nm-650 nm wavelength.
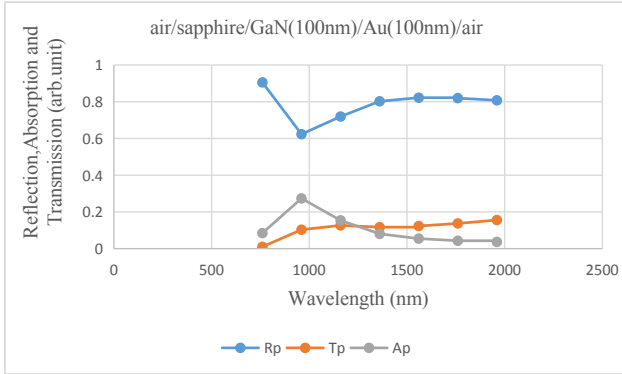
Figure 21. Absorption Analysis on Short Wave Wavelength

Figure 21 shows reflection, absorption and transmission value in short wave wavelength (760 nm-1960 nm). Reflection (R_p) value is inversely proportional to absorption (A_p) value. But transmission (T_p) value is almost inversely proportional absorption (A_p).

Reflection, absorption and transmission value in medium wave (2000 nm-4000 nm) is shown in Figure 22.
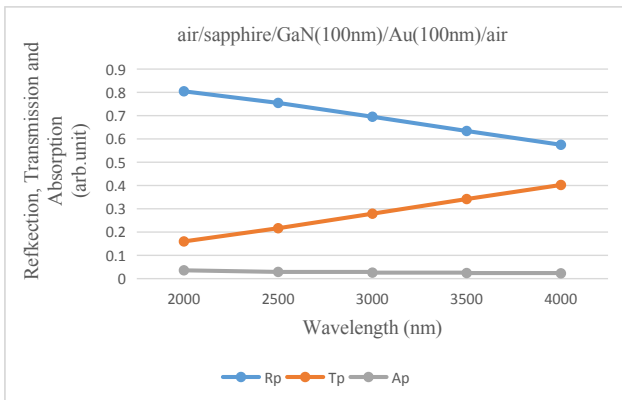
Figure 22. Absorption Analysis on Medium Wave Wavelength

Medium wave reflection (R_p) value is lower than short wave R_p value. Medium wave transmission (T_p) value is higher than short wave T_p value. Reflection (R_p) is inversely proportional to transmission (T_p) value. And Medium wave absorption (A_p) value is low in this condition.
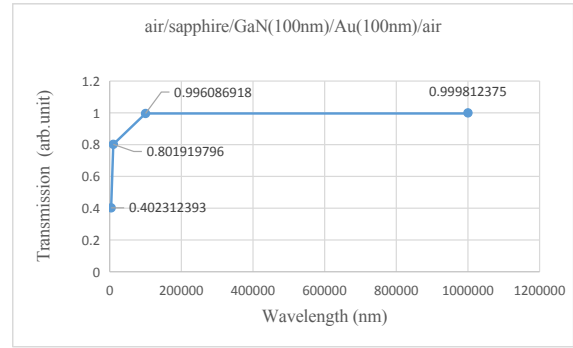
Figure 23. Transmission on Long Wave Wavelength

Figure 25 describes the reflection, absorption and transmission value in long wave wavelength (4000 nm-1000000 nm). Long wave reflection (R_p) value is lower than medium wave R_p value. Long wave transmission (T_p) value is higher than medium wave T_p value.

And long wave absorption (A_p) value is lower than medium condition and absorption value is nearly close to zero in this wavelength.
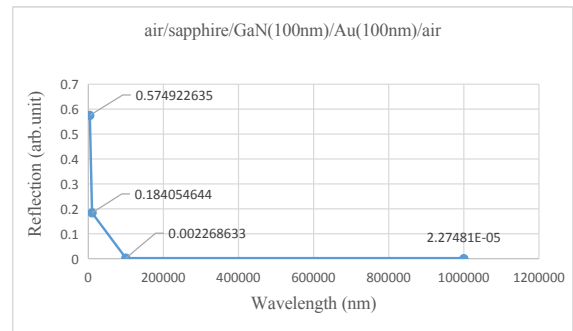
Figure 24. Reflection on Long Wave Wavelength
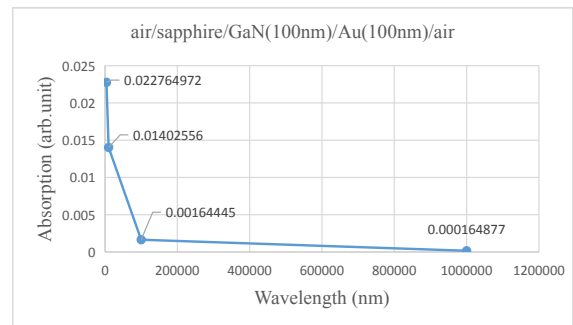
Figure 25. Absorption Analysis on Long Wave Wavelength

Absorption coefficient value is very important for optical semiconductor devices because heat in these devices is occurred in absorption of light in materials.

3.3 Transmission, Reflection and Absorption Analysis on S-Polarized Incident Angle

Reflection, transmission and absorption values for air/

sapphire/GaN/Au/air structure along the s-polarized angle of incidence 10 to 90 degrees is shown in Figure 26. When the reflection value is high, the transmission value is low in this structure. Absorption value is higher than transmission value for this condition.
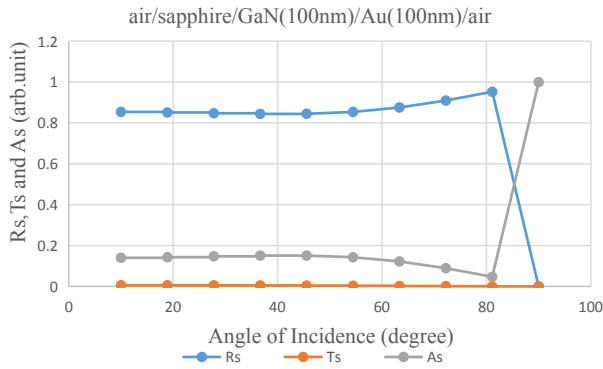
Figure 26. Reflection, Transmission and Absorption Analysis

Along the s-polarized angle of incidence, 81 degree incident light is the highest reflection value otherwise this condition gets low absorption rate.

3.3.1 Analysis on Thickness of Materials

The 80 degree s-polarization of light is incident on this metal-semiconductor structure. The thickness of Au (10 nm to 100 nm) metal result is shown in Figure 27. 100 nm thick Au metal has high reflection value. Transmission value is zero and absorption value is nearly 0.14. So, s-polarization of 100 nm or upper thickness of Au metal layer gets more absorption value than p-polarization of Au metal layer.

Inversely proportional of reflection and absorption values can be seen in this result. Transmission value is nearly zero value in this condition. So, 100 nm or upper thickness of GaN semiconductor layer should be used in high performance device (for less phonon effect).
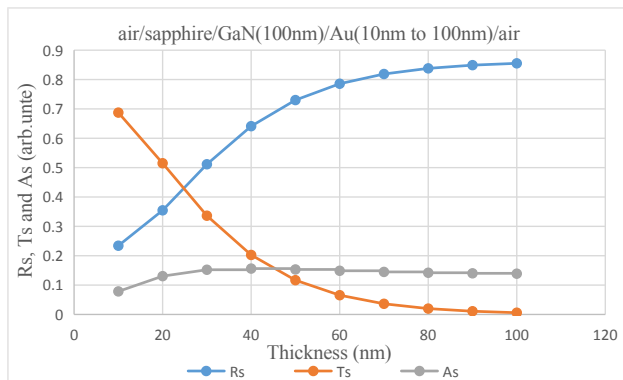
Figure 27. Reflection, Transmission and Absorption Analysis of Metal Layer

The semiconductor GaN (10nm to 100 nm) layer thickness changes result is shown in Figure 28.
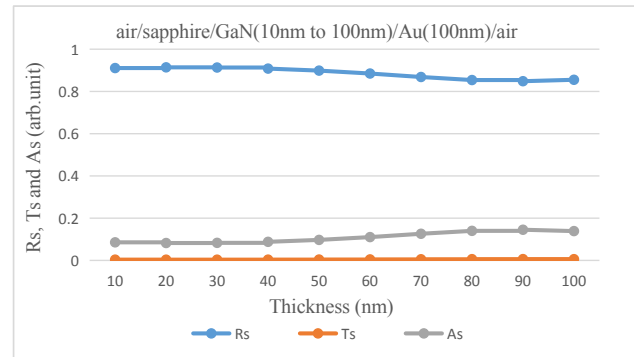
Figure 28. Reflection, Transmission and Absorption Analysis of Semiconductor Layer

3.3.2 Absorption Analysis on IR Wavelength

Figure 29 shows reflection, absorption and transmission value in short wave wavelength (760 nm-1960 nm).
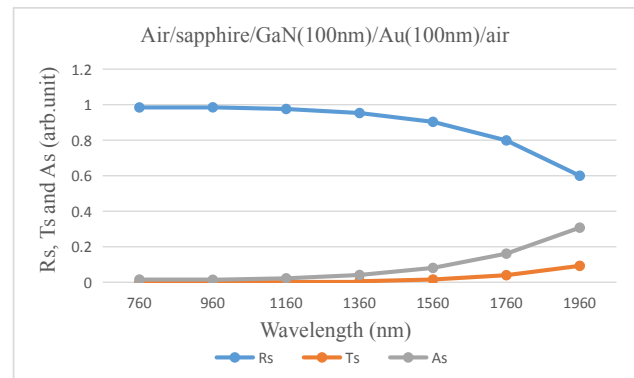
Figure 29. Absorption Analysis on Short Wave Wavelength

Reflection (R_s) value is inversely proportional to absorption (A_s) value. Transmission (T_s) value is lower than absorption (A_s) in s-polarized light. Reflection, absorption and transmission value in medium wave (2000 nm-4000 nm) is shown in Figure 30.
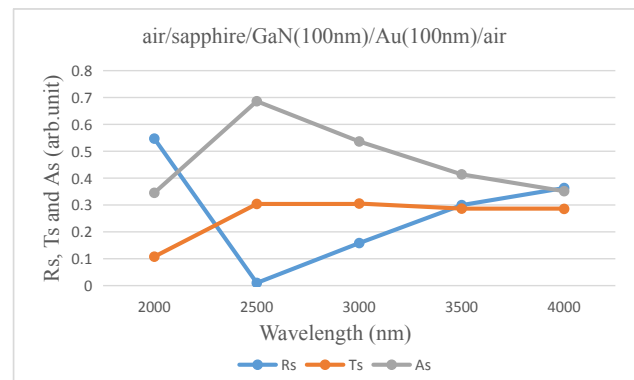
Figure 30. Absorption Analysis on Medium Wave Wavelength

Medium wave reflection (R_s) value is lower than short wave R_s value. Medium wave transmission (T_s) value is higher than short wave (T_s) value. Reflection (R_s) is inversely proportional to absorption (A_s) value. And Medium wave absorption (A_s) value is high in this condition.
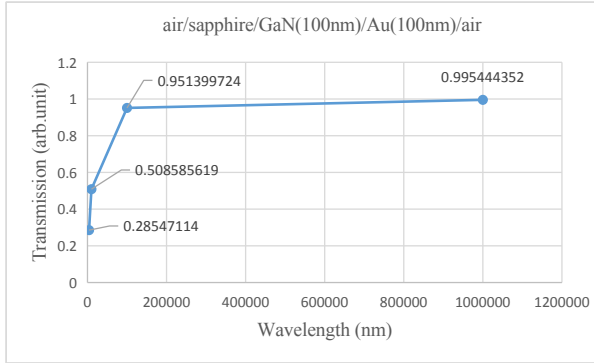
Figure 31. Transmission on Long Wave Wavelength

Figure 31, 32 and 33 describe the transmission, reflection, and absorption value in long wave wavelength (4000 nm-1000000 nm).
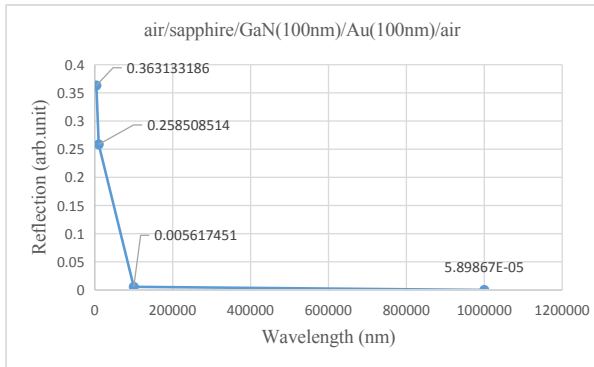
Figure 32. Reflection on Long Wave Wavelength

Long wave reflection (R_s) value is lower than medium wave R_s value. Long wave transmission (T_s) value is higher than medium wave T_s value. And long wave absorption (A_s) value is lower than medium condition and absorption value is nearly close to zero in this wavelength.
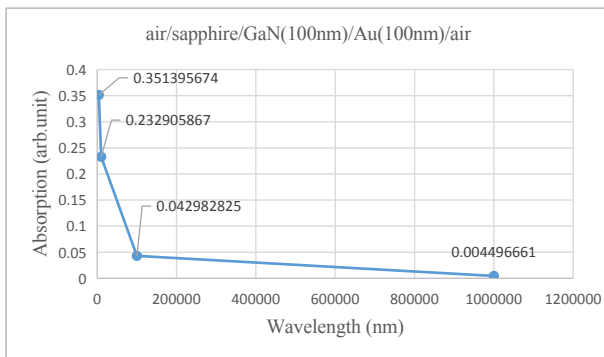
Figure 33. Absorption Analysis on Long Wave Wavelength

Absorption coefficient value is very important for optical semiconductor devices because heat in these devices is occurred in absorption of light in materials.

3.4 FDTD Absorbing Boundary Condition for Semiconductor Quantum Devices

The FDTD simulation for e-field and transmission coefficients for time steps =500 is illustrated in Figure 34. There are many simulation approaches for transmission and reflection condition for electromagnetic energy through the medium like PML boundary or MUR boundary. The simulation results show that the FDTD analysis on absorbing boundary condition for semiconductor quantum devices can be focused on the optical properties of the devices for high performance condition.

(a)

(b)
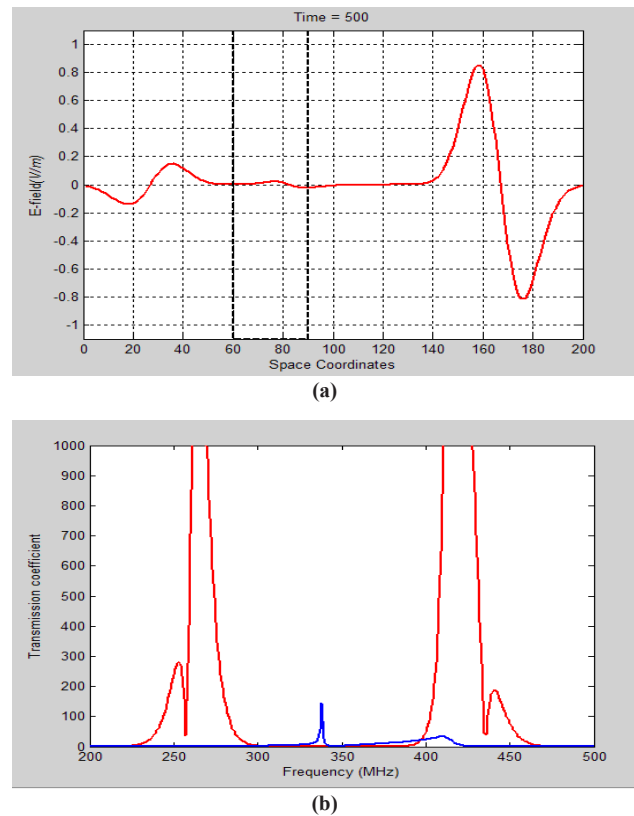
Figure 34. FDTD Simulation for (a) E-field and (b) Transmission Coefficients for Time Steps = 500

Figure 35 shows the reflection pulse at metal-semiconductor interface with MUR ABC boundary. Depending on the boundary condition, the reflection center is occurred at 250 microns in x-coordinate in MUR analysis with FDTD simulation between metal and semiconductor interface.
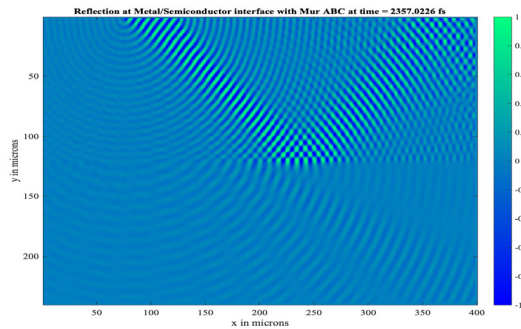
Figure 35. Reflection Pulse at Metal/Semiconductor Interface with MUR ABC Boundary

The reflection pulse can be detected 400 microns in x-coordinate and it is the best detection point for the carrier dynamics effects for interface engineering. Figure 36 shows the transmission pulse at metal-semiconductor interface with MUR ABC boundary.
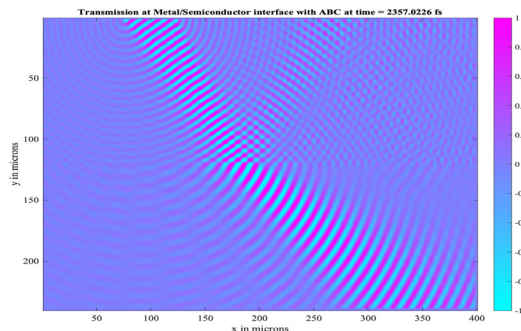
Figure 36. Transmission Pulse at Metal/Semiconductor Interface with MUR ABC

Resting on the boundary condition, the transmission midpoint is occurred at 180 microns in x coordinate in MUR investigation with FDTD simulation between metal and semiconductor interface. The reflection pulse can be detected 350 microns in x coordinate and it is the finest detection point for the carrier dynamics effects for interface engineering.

Figure 37 shows the reflection pulse at metal-semiconductor interface with PML boundary.
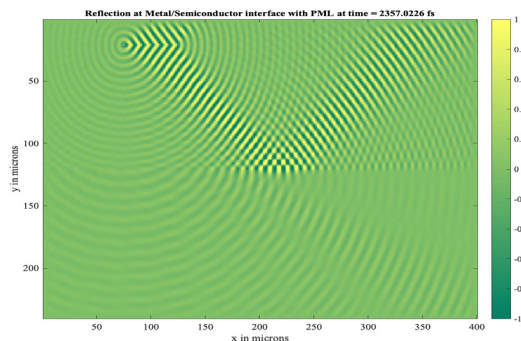
Figure 37. Reflection Pulse at Metal/Semiconductor Interface with PML Boundary

Based on the boundary condition of PML, the reflection center is transpired at 225 microns in x coordinate in PML analysis with FDTD simulation between metal and semiconductor interface. The reflection pulse can be identified 350 microns in x coordinate and it is the paramount recognition point for the carrier dynamics effects for interface engineering.

Figure 38. Transmission Pulse at Metal/Semiconductor Interface with PML Boundary

Figure 38 shows the transmission pulse at metal-semiconductor interface with PML boundary. Established on the boundary condition of PML, the transmission focus is emerged at 160 microns in x coordinate in PML analysis with FDTD simulation between metal and semiconductor interface.

3.5 Discussions

Finite-Difference Time-Domain analysis on absorbing boundary condition for solving a time-dependent Schrödinger equations are studied. The reflectance and transmittance energy from Au/GaN interface, the electric field and electric flux density value are obtained at the metal-semiconductor interface. The measurement on reflection value of gold, platinum and titanium metal is coated on GaN semiconductor with 100 nm thickness. One dimensional FDTD method is one of the solutions for observing the energy spectrum in a semiconductor material. These simulation researches tend to fabricate the photodetectors or other device to get the better performance of metal-semiconductor based optical semiconductor devices. This study affects to find the new solution for less phonon energy (or) small absorption measurement on metal-semiconductor layer structure. That practice can solve a discretized Schrödinger equation in an iterative progression. The comprehensive FDTD method is experienced by simulating a particle stirring in free space and then trouncing an energy potential. Numerical results correspond to attain based on the outcomes from the simulation results.

The short, medium and long IR wavelengths of the Au/GaN samples were studied by affecting the winspall technique. The absorption value for Au/GaN sample was described with p-polarization and s-polarization of IR light. P-polarization light absorption value is smaller than s-polarization light absorption value. But reflection value is high in both p-polarization and s-polarization. Less absorption value device structure can protect the rising of heat in processing of this device. So, Au/GaN structure is less phonon effect structure for fabricating of metal-semiconductor based semiconductor device such as photodetectors. The transmittance and reflectance spectra on three metals is confirmed by winspall techniques which depend on the absorption spectrum. The transmittance and reflectance spectrum for interface of metal-semiconductor are also described with finite-difference time domain method by Mur's and PML (perfectly matched layer) boundary conditions. Perfectly matched layer boundary condition can early detect the sharp signal than the Mur's absorbing boundary condition. Conduction band energy or electron concentration of these structure models are compared with the Schrodinger model and conventional model. The junction capacitances due to dipole in the transition region are also illustrated under reverse bias condition.

4. Conclusions

A comprehensive FDTD method has developed with various kinds of absorbing boundary condition for solving the 1D time dependent Schrödinger equation and obtains a more relaxed condition for stability when central difference calculations are presented in new physical results, the power of the FDTD technique must be borne in mind. As an explicit space-domain technique, one can avoid difficulties associated with constructing single-particle orbital that is used in computations based on Slater determinate. A Slater-determinant-based calculation will require computing the single-particle orbital for each potential chosen. Of course, the trade-off is in the size of the spatial mesh chosen for calculations.

Low absorption based device structure is suitable for high performance device because this structure can fabricate less phonon effect device structure. The simulation results have been conducted by using MATLAB language for analysis. A comparison of the phonon energy with the p-polarization and s-polarization as measured by absorption and reflection value shows that the short, medium and long wave IR wavelength. In short wave, s-polarized IR light absorption value is higher than p-polarized IR light absorption value. In medium wave, s-polarized IR light absorption value is also higher than p-polarized IR light absorption value. Long wave absorption result is also the same above phenomenon. But reflection or transmission value is always high along the whole IR wavelength.

References

[1] Lee, Y. S. 2009. "Principles of Terahertz Science and Technology."

[2] Jacobsen, F.2008. "An Efficient Realization of Frequency Dependent Boundary Conditions in an Acoustic Finite-Difference Time-Domain Model." vol. 316: 234-247.

[3] Chatterjee, S.2004. "Excitonic Photoluminescence in Semiconductor Quantum Wells: Plasma versus Excitons." Physical Review Letters, vol.92, issue.6.

[4] Koch, S. W. 2011. "Semiconductor Quantum Optics." Cambridge University Press.

[5] Li, W. 2006. "Post Growth Thermal Annealing of GaN Grown by RF Plasma." Journal of Crystal Growth, vol.227 : 415-419.

[6] Khromov, S. 2013. "Doping Effects on the Structural and Optical Properties of GaN." Science and Technology Dissertation, no. 1554, Sweden: Thin Film Physics.

[7] Bengtsson, M. 2008. "Finite Difference Time-Domain Simulations of Exciton-Polariton Resonances in Quantum Dot Arrays." Optical Society of America, vol.16, no. 7 : 4507-4519.

[8] Lee, Y. S. 2009. "Principles of Terahertz Science and Technology."

[9] Moini, M. 2008. "On the Numerical Solution of One Dimensional Schrödinger Equation with Boundary Conditions Involving Fractional Differential Operators." International Journal of Engineering Science, vol.19 : 21-26.